Solar Energy 135 (2016) 59–69

Contents lists available at ScienceDirect

Solar Energy

journal homepage: www.elsevier.com/locate/solener

Optimal control of a fuel cell/wind/PV/grid hybrid system with thermal heat pump load

Sam Sichilalu [a,*], Henerica Tazvinga [b], Xiaohua Xia [a]

[a] Centre of New Energy Systems, Department of Electrical, Electronic and Computer Engineering, University of Pretoria, Pretoria 0002, South Africa
[b] Energy Centre, Council for Scientific and Industrial Research, P.O. Box 395, Pretoria 0001, South Africa

ARTICLE INFO

Article history:
Received 9 February 2016
Received in revised form 15 May 2016
Accepted 18 May 2016

Keywords:
Fuel cell
Heat pump water heater
Optimal control
Dispatch strategy
Wind generator
Photovoltaics
Electrolyzer
Energy feed-in

ABSTRACT

This paper presents an optimal energy management strategy for a grid-tied photovoltaic–wind-fuel cell hybrid power supply system. The hybrid system meets the load demand consisting of an electrical load and a heat pump water heater supplying thermal load. The objective is to minimize energy cost and maximize fuel cell output, taking into account the time-of-use electricity tariff. The optimal control problem is solved using a mixed binary and real linear programming. The supply switch to the heat pump water heater and the power from the grid, power to/from the inverter, electrolyzer hydrogen power and fuel cell power are the control variables. The temperature inside the water storage tank and the hydrogen in the storage tank are the state variables. The performance of the proposed control strategy is tested by simulating different operating scenarios, with and without renewable energy feed-in or rather export to the grid, and the results confirm its effectiveness, as it increases the supply reliability of the system.

1. Introduction

Rising costs, depletion and environmental concerns about fossil fuel-based energy resources have led to significant research effort in renewable and cleaner energy resources. Globally, governments are adopting policies to promote the development and application of various renewable energy (RE) technologies for generating electricity. The main challenge associated with RE technologies such as solar and wind generator is their intermittent nature, which affects their ability to provide 100% supply reliability. Combining these RE sources with battery storage and diesel generator systems has been shown in various studies to be cost-effective (Hove and Tazvinga, 2012; Dufo-Lopez et al., 2011; Tazvinga et al., 2015). Currently there are limitations to the fraction of RE (wind and solar) that can be incorporated in the grid system because of their intermittency and base load considerations. With the latest developments pointing towards the feasibility of the hydrogen economy, solar and wind power fractions can be safely extended within the grid system by compensating for their intermittency with an energy storage medium such as hydrogen. Interest in hydrogen is mainly driven by its ability to reduce carbon dioxide emissions, thereby helping to mitigate climate change, improve local air quality, improve energy security by reducing energy imports, increase energy supply options, reduce dependence on fossil fuels, and contribute to the introduction of advanced fuel cell (FC) technologies with high efficiency.

FCs are promising sources of electricity that are environmentally friendly. Use of hydrogen FCs for power production is receiving a lot of interest in many research communities, with industrial applications in automobile industries and heat pumps (Ellis et al., 2001). FCs can serve as emergency sources of energy in the event of a long-term power outage and in stand-alone applications. They are replacing battery systems and are increasingly being used in distributed generation systems. Hydrogen, once produced and stored, can generate power on demand. In order for photovoltaic (PV) and wind systems to meet demand completely, there is a need for backup systems such as diesel generators (DGs), hydrogen FCs and battery storage in a hybrid system (Wang et al., 2016; Reihani et al., 2016; Feng et al., 2015; Purvins and Sumner, 2013). Hybrid energy systems present a solution to the time correlation of intermittent RE sources (Ranaboldo et al., 2015; Tazvinga et al., 2013). RE-based power systems are being deployed globally to provide autonomous power for various remote applications and also in grid-tied systems. Improvements in the performance of these systems for both grid and off-grid applications continue globally in many research communities (Bouzerdoum et al., 2013).

* Corresponding author.
E-mail addresses: Sam.Sichilalu@up.ac.za, sichgroup@yahoo.com (S. Sichilalu).

http://dx.doi.org/10.1016/j.solener.2016.05.028
0038-092X/

Nomenclature

$P_{w,t}$	wind generator power output (kW)
$P_{pv,t}$	photovoltaic power output (kW)
$P_{g,t}$	grid power (kW)
$P_{hp,t}$	heat pump water heater rated power (kW)
$P_{RE-IN,t}$	direct renewable power supply (kW)
$P_{el,t}$	power supply to the electrolyzer (kW)
$P_{H2,t}$	eletrolyzer hydrogen power output (kW)
$H_{2,t}$	stored hydrogen energy (kWh)
$P_{FC-IN,t}$	fuel cell power output (kW)
$P_{\text{Load,t}}$	domestic load (kW)
$P_{FC,t}$	hydrogen power input to the fuel cell (kW)
COP	coefficient of performance
u_t	heat pump power supply switch control variable (0 or 1)
T_t	hot water temperature inside the tank (°C)
T_{low} and T_{up}	lower and upper hot water temperature set points (°C)
T_a	ambient temperature (°C)
T_o	initial hot water temperature (°C)
$T_{in,t}$	inlet cold water temperature (°C)
R	South African rands (1R = 0.074 USD as of 22.09.2015)
$\lambda_{(t)}$	time-of-use electricity price (R/kWh)
N	total number of sampling intervals
t_s and k	sampling time (*hour*) and kth sampling interval respectively
J	cost function
Q_D	total losses due to water demand
Q_L	total standby (convectional) losses
$W_{D,t}$	flow rate (liters/hour)
q_{loss}	conventional loss in (W/m^2)
$\triangle x$	thickness of the insulation (m)
h	surface heat transfer coefficient (W/m^2 K)
κ	thermal conductivity (W/m K)
S_{area}	total surface area (m^2)
c	specific heat capacity of water (J/kg °C)
ø	diameter (m)
$\dot{T}$	derivative of temperature
L	mass of water inside the tank (kg)
h_{ref}	anemometer reference height (m)
φ	ground surface friction coefficient
v_{hub}	wind speed at the desired height h_{hub}
v_{ref}	wind speed at the reference height h_{ref}
V	wind speed at the hub height (m/s)
χ	Weibull shape parameter
P_r	rated wind electrical power (kW)
V_{in}	cut-in wind speed (m/s)
V_r	rated wind speed (m/s)
V_{out}	cut-off wind speed (m/s)
MILP	mixed integer linear program
TOU	time-of-use electricity tariff
Eskom	South African power utility company

Various energy management strategies have been proposed for different hybrid system configurations (Choudar et al., 2015; Korpås and Holen, 2006; Tazvinga et al., 2014). A standalone RE/FC hybrid system that uses at least one RE source and a polymer electrolyte membrane (PEM) FC as backup source is analyzed in Bizon et al. (2015). Frequency fluctuation analysis of a wind, DG and FC hybrid power system connected to a local utility point has been presented in Singh et al. (2015) and the results show that the FC system can give better performance for stabilizing the frequency of the system in comparison to DGs. Electrochemical energy storage systems such as hydrogen systems can offer sufficient flexibility for operation in connection with stochastic generation from wind and PV and local energy storage can also increase the exploitation of the energy source (Korpås and Holen, 2006). Use of hydrogen as a storage medium for variable energy sources is a promising alternative in the long run, since it can be used as a clean fuel in the transport sector and for power production in stationary FCs (Korpås and Holen, 2006; Bizon et al., 2015).

It is important to note that energy consumption in buildings, especially in developed countries, accounts for close to 42% of global energy production and 60.51% of this energy is used for space heating, while 23.60% goes for water heating at domestic level (Rahman et al., 2010; Chow et al., 2012; Zhang et al., 2013). Therefore, only energy-efficient equipment such as heat pump water heaters (HPWH) should be used to produce the much needed thermal energy. The use of HPWHs in demand side management (DSM) yields more benefit than its counterpart, cylinder hot water heaters, owing to its coefficient of performance (COP). Great success in optimal design and control of HPWHs in the last decades has increased their application even at domestic level (Chua et al., 2010). Safdarian mentioned that domestic heating systems has a potential for DSM (Safdarian et al., 2016; Seo et al., 2014). HPWHs have advantages such as they could be applied in heating, ventilation, and air-conditioning (HVAC) systems (Fabrizio et al., 2014; Huang et al., 2006; Arteconi et al., 2013; Kilkis, 1999). Nevertheless there are still a few drawbacks, such as heating water to the required temperature in a short time and the initial investment cost (Verhelst et al., 2012; Rousseau and Greyvenstein, 2000). RE integration with such energy-efficient equipment is in its infancy stage (Roonprasang et al., 2008; Sichilalu and Xia, 2015; Sichilalu et al., 2015).

In most of the work done by various researchers, DGs and battery storage are the common power back-up in RE hybrid systems, instead of greener hydrogen FCs. The main focus in FC technology has been the evaluation of performance index on life cycle cost, optimal sizing and hybridization only (Rodatz et al., 2005; Pukrushpan et al., 2004; Pukrushpan et al., 2002) rather than optimal control (OC). While most of these back-up systems, (e.g. DGs) are expensive to run and have negative environmental effects. Though FCs technology seems to have a high initial investment cost, it is in fact cheaper and greener in the long term. This paper presents a first-ever OC strategy model on an integrated RE-FC-grid system with an energy-efficient thermal load under a time-of-use (TOU) tariff. This model presents a practical FC feed-in OC strategy. This paper simulates a 24-h control horizon, giving a comprehensive hourly energy usage pattern and its implications. Often customers do not change their energy usage behavior because of lack of detailed short-period energy consumption/bill correlation in the accumulative monthly bill.

This paper is structured as follows: Sections 2 present the mathematical model formulation and Section 3 the simulation results and discussion. The last part, Section 4, is the conclusion.

2. Mathematical model formulation

2.1. Schematic diagram of the model

The schematic layout is shown in Fig. 1. The PV modules $P_{pv,t}$ and wind generator $P_{w,t}$ feed through their respective inverters into the direct current (DC) bus. The DC bus then supplies through $P_{RE-IN,t}$ to the loads and the other $P_{el,t}$ to the FCs electrolyzer for the generation of hydrogen. The generated hydrogen, $P_{H2,t}$, is stored in the hydrogen storage tank, H_2, which later supplies

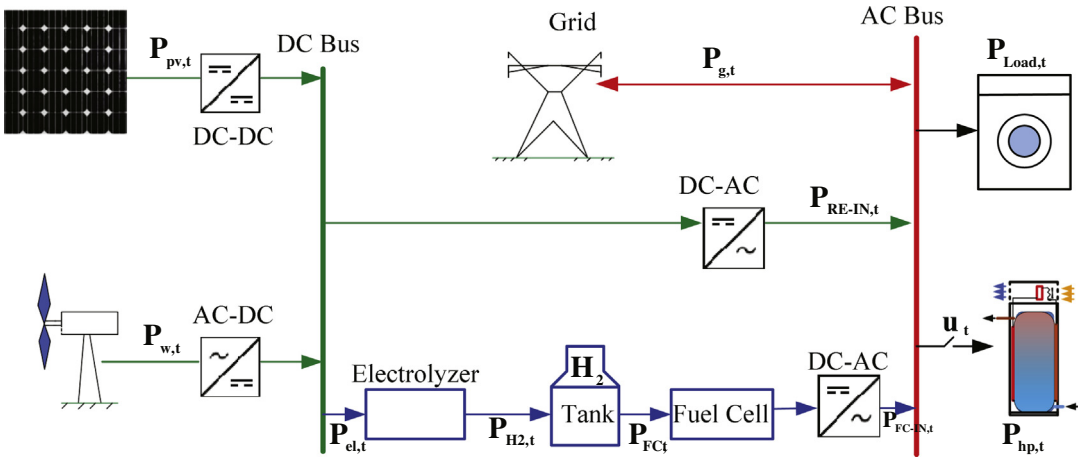

Fig. 1. Schematic layout diagram of the proposed fuel cell/wind/PV/grid hybrid system with both loads.

hydrogen, $P_{FC,t}$, to the FC. The FC output is rectified and feeds into the grid alternating current (AC) bus through $P_{FC-IN,t}$ where the loads are connected.

The grid power, $P_{g,t}$, supplies the load via the AC bus direct with a possibility of REs feed-in. The domestic load $P_{\text{Load},t}$ represent all other loads in the building apart from the thermal loads. The thermal load considered in this model is the heat pump water heater because of its high energy-efficiency. The heat pump, $P_{hp,t}$, works at full load at its rated power whenever it is in operation, and is controlled by switch u_t. The control variables are $P_{RE-IN,t}, P_{el,t}, P_{H2,t}, P_{FC,t}, P_{FC-IN,t}, P_{g,t}$ and switch u_t. The state of hydrogen energy in the tank $H_{2,t}$ and the heat pump's hot water temperature T_t are the two state variables.

The system above is further subdivided into their respective mathematical models.

2.2. Heat pump water heater

The heat pump model is developed according to Sichilalu et al. (2015) and Kim et al. (2004), with a fixed power demand P_{hp} rating, operating at full capacity. The hot water temperature distribution inside the tank is treated as uniform. For modeling simplicity, the energy losses in the evaporator, refrigerant and compressor are neglected. The COP depicts the thermal equipment efficiency and is assumed to be constant, as given in the case study, though in practice it varies depending on input values. In this model, only energy losses due to hot water demand $Q_{D,t}$ and convectional (standby) loss $Q_{L,t}$ are modeled.

The standby losses, $Q_{L,t}$, represent power losses owing to the casing material surface conduction. The per second convention loss q_{loss} in W/m^2, according to Zhang and Xia (2007), is given in Eq. (1),

$$q_{loss}(T_t, T_a) = \frac{T_t - T_a}{\frac{\Delta x}{\kappa} + \frac{1}{h}}, \tag{1}$$

where Δx and κ are the insulation thickness and thermal conductivity coefficients respectively, h is the surface heat transfer coefficient of the tank, while T_t and T_a are the hot water and ambient temperatures respectively. A given tank surface area, S_{area}, has a total standby loss of:

$$Q_L(T_t, T_a) = q_{loss} S_{area}. \tag{2}$$

The other loss is due to the hot water demand $Q_{D,t}$, allowing inlet cold water. Consequently, every time demand occurs T_t drops and inlet of cold water proportionally flows into the tank, keeping a constant volume. Losses due to the hot water demand are given as (Khan et al., 2004; Gustafson et al., 1993):

$$Q_{D,t} = cW_{D,t}(T_t - T_{in}), \tag{3}$$

where $c = 4180 J/kg/^{\circ}C$ is the specific heat capacity of water. T_{in} is the municipal inlet water temperature whereas $W_{D,t}$ is the hot water demand flow rate in liters/hour.

The HPWH thermal output requirements and the corresponding electrical power input is given by Ji et al. (2005) and Khan et al. (2004):

$$P_{hp,t} = \frac{Q_{D,t} + Q_{L,t}}{COP}. \tag{4}$$

The power balance is a dynamic equation. Let $Q_{H,t}$ be the total HPWH heat output kilowatts and L the water mass (tank capacity) in kilograms. Then the power balance becomes a first derivative differential function given in Eq. (5) (Dolan et al., 1996).

$$cL\dot{T}_t = Q_{H,t} - Q_{L,t} - Q_{D,t}, \tag{5}$$

$$Q_{H,t} = P_{hp} COP u_t. \tag{6}$$

By substituting Eqs. (1)–(4) into Eq. (5), one gets

$$\dot{T}_t = \frac{P_{hp} COP u_t - S_{area}\left(\frac{T_t - T_a}{\frac{\Delta x}{\kappa} + \frac{1}{h}}\right) - cW_{D,t}(T_t - T_{in,t})}{cL}, \tag{7}$$

denoting:

$$\alpha_t = \frac{S_{area}}{cL\left(\frac{\Delta x}{\kappa} + \frac{1}{h}\right)} + \frac{W_{D,t}}{L}, \tag{8}$$

$$\beta = \frac{P_{hp} COP}{cL}, \tag{9}$$

$$\gamma_t = \frac{S_{area} T_a}{cL\left(\frac{\Delta x}{\kappa} + \frac{1}{h}\right)} + \frac{W_{D,t} T_{in,t}}{L}, \tag{10}$$

then Eq. (7) becomes:

$$\dot{T}_t = -\alpha_t T_t + \beta u_t + \gamma_t. \tag{11}$$

2.3. Wind generator

The power output of a wind turbine at a given site depends on wind velocity at hub height and turbine speed characteristics. The standard height or reference for wind speed measurements for wind resource assessment is usually 10 m above the effective ground level, therefore it is necessary to determine the wind speed at hub height. This is important because it is the wind speed experienced by the rotor of the wind turbine (hub height wind speed)

that determines the actual power radiated by a particular turbine. The most common expression used for this purpose is the power-law equation, expressed as (Belfkira et al., 2011; Patel, 2006; Tazvinga et al., 2014; Li et al., 2009):

$$v_{hub} = v_{ref} \cdot \left(\frac{h_{hub}}{h_{ref}}\right)^{\varphi}, \tag{12}$$

where v_{hub} is the wind speed at the desired height h_{hub}, v_{ref} is the wind speed at the reference height h_{ref} and φ is the power law exponent, which represents the ground surface friction coefficient. The exponent is a function of height, time of day, season, nature of the terrain, wind speed, and temperature. It is low for smooth terrains, high for rough terrains and the values for typical classes are given in Patel (2006). The coefficient ranges from $\frac{1}{7}$ to $\frac{1}{4}$. $\frac{1}{7}$ is used in this work, which is typical for open land. The v_{hub} obtained is then used in the wind power equation. The power output of a wind turbine thus depends on the wind speed pattern at the specific location, air density, rotor swept area and energy conversion efficiency from wind to electrical energy.

The hub height velocity is used in the output power model to calculate the power generated by the wind turbine generator. The models used to describe the performance of wind generator (WG) are different since different WGs have different power output performance curves. Various models are used to simulate the wind turbine power output (Ashok, 2007; Patel, 2006). Various authors have developed different models for calculating the power output by making various assumptions and assuming that the turbine power curve has a linear, quadratic or cubic form (Lu et al., 2002; Bueno and Carta, 2005). The general expression used is as follows:

$$P_w = \begin{cases} P_r \frac{V^{\chi} - V_{in}^{\chi}}{V_r^{\chi} - V_{in}^{\chi}}, & (V_{in} \leqslant V \leqslant V_r) \\ P_r, & (V_r \leqslant V \leqslant V_{out}) \\ 0, & (0 \leqslant V_{in} \text{ and } V \leqslant V_{out}) \end{cases} \tag{13}$$

where V is the wind speed at the hub height, χ is the Weibull shape parameter taken as 2 in this paper, P_r is the rated electrical power; V_{in} is the cut-in wind speed; V_r is the rated wind speed and V_{out} is the cut-off wind speed. The wind model parameters are presented in the case study as given in Table 2.

2.4. Hydrogen fuel cell

The hydrogen storage system consists of an electrolyzer and hydrogen storage tank. The input energy for the electrolyzer is supplied by the RE sources during periods of excess production for hydrogen production by water electrolysis and is stored in the tank to be used by the FC during periods when the energy produced by the RE sources is not enough to meet the load. The storage tank is operated within the maximum and minimum levels of hydrogen storage and a minimum amount of hydrogen should remain in the tank to maintain a security limit. The electrolyzer is connected directly to the hydrogen tank and power from the electrolyzer to the tank, $P_{el,t}$, is given by:

$$P_{el,t}\eta_{el} = P_{H2,t}, \tag{14}$$

where $P_{el,t}$ is the renewable power input to the electrolyzer, $P_{H2,t}$ is the hydrogen power output and η_{el} is the efficiency of the electrolyzer and is assumed to be constant. The energy in the hydrogen storage tank at any given time is expressed as:

$$\dot{E}_{s,t} = P_{H2,t} - \frac{1}{\eta_s} P_{FC,t} \tag{15}$$

in which, η_s is the storage discharging efficiency taken as 95% owing to leakages and pumping (Wallmark and Alvfors, 2002). The following general expression thus applies to the storage dynamics in discrete time with a sampling time, t_s:

$$E_{s,t} = E_s(0) + \sum_{\tau=1}^{t} P_{H2,\tau} t_s - \frac{1}{\eta_s} \sum_{\tau=1}^{t} P_{FC,\tau} t_s, \tag{16}$$

where $E_s(0)$ is regarded as the initial SOC of the storage tank.

$P_{H2,\tau}$ is the power accepted by the storage at time t, and $\frac{1}{\eta_s}\sum_{\tau=1}^{t} P_{FC,\tau}$ is the power drawn from the storage at time t. The mass of hydrogen stored in the tank at any given time t is given by:

$$Mass_{h,t} = \frac{E_{s,t}}{HHV_h}, \tag{17}$$

where HHV_h is the higher heating value of hydrogen equal to 39.7 kWh/kg (Korpås and Holen, 2006; Kaviani et al., 2009). The storage operates within maximum and minimum limits.

FC stacks produce direct current at a voltage that varies with the load. A switching power converter is used to match the voltage produced by the FC to the needs of the application and to protect the FC from over-current or under-voltage conditions. In this work the application requires AC, so the electricity is then processed through a DC/AC inverter. FCs also produce thermal energy but this is not considered in this work. There are various types of FCs and in this work the proton exchange membrane FC is considered owing to its reliable performance under variable supply and its availability in a wide range of capacities. The output power, $P_{FC-IN,t}$ is a function of the input power, $P_{FC,t}$, and FC efficiency η_{FC} (assumed constant) given by:

$$P_{FC-IN,t} = \eta_{FC} P_{FC,t}. \tag{18}$$

The FC output is restricted within:

$$E^{min} \leqslant E_{s,t} \leqslant E^{max}. \tag{19}$$

2.5. Photovoltaic power

The PV power output profile $P_{pv}(t)$ is input data, taken from the case study in our previous research (Sichilalu and Xia, 2015; Tazvinga et al., 2013). The PV power input data are given in Fig. 4.

2.6. Grid power

The grid is capable of accepting and supplying power to the AC bus where the load is connected. TOU electricity tariff (dynamic pricing) is an important control parameter in a load-shifting strategy. In South Africa the main power utility is called Eskom. Because of a high power deficit and aging infrastructure, dynamic pricing was introduced to level the load and discourage peak period power consumption. The pricing $\lambda_{(t)}$ model is: off-peak (λ_o), standard (λ_s) and peak (λ_p). The recent Eskom[1] megaflex active energy-TOU tariff is adopted in this model. The TOU tariff is:

$$\lambda_{(t)} = \begin{cases} \lambda_o = 0.3656R/\text{kWh} & \text{if } t \in [0,7] \cup [23,24], \\ \lambda_s = 0.6733R/\text{kWh} & \text{if } t \in [7,8] \cup [11,19] \cup [21,23], \\ \lambda_p = 2.2225R/\text{kWh} & \text{if } t \in [8,11] \cup [19,21], \end{cases} \tag{20}$$

where R is the South African rand and t is the time of day with $t = 0, \ldots, 23$.

The feed-in tariff is regulated by the National Energy Regulator of South Africa (NERSA).[2] NERSA, through the renewable energy purchasing agency, is the single buyer office of Eskom, guaranteeing

[1] http://www.eskom.co.za/.
[2] http://www.nersa.org.za/.

the renewable energy market. The prevailing PV feed-in tariff is 3.94*R*/kWh, whereas for wind it is 1.25*R*/kWh.

2.7. DC and AC bus power balance

The power balance at the DC bus is given as:

$$P_{el,t} + P_{RE-IN,t}/\eta_{in} = P_{w,t}\eta_w + P_{pv,t}\eta_{pv}, \tag{21}$$

where $P_{el,t}$ is the renewable power input to the electrolyzer and $P_{RE-IN,t}$ is the direct renewable energy power supply to the loads. η_{in}, η_w and η_{pv} are the efficiency of the DC/AC, wind generator and PV inverters respectively.

The power balance at the AC load bus is given as:

$$P_{g,t} + P_{RE-IN,t} + P_{FC-IN,t} = P_{\text{Load},t} + P_{hp,t}u_t, \tag{22}$$

where $P_{g,t}$ is the grid power,and $P_{FC-IN,t}$ is the FC power output. $P_{\text{Load},t}$ and $P_{hp,t}u_t$ are the domestic load and heat pump demand respectively, whereas u_t is the heat pump's power supply switch.

2.8. Formulation of a discretized hot water model

The water demand flow rate $W_{D,t}$ and the inlet water, $T_{in,t}$, are functions of time as presented in the case study section in this paper. The general discrete formulation of Eq. (11) in terms of the k-th hot water temperature is given in Eq. (23):

$$T_{k+1} = (1 - t_s\alpha_k)T_k + t_s\beta u_k + t_s\gamma_k. \tag{23}$$

Then, T_{k+1} at each interval can be derived as:

$$\begin{aligned}
T_1 &= (1 - t_s\alpha_0)T_o + t_s\beta u_0 + t_s\gamma_0,\\
T_2 &= [(1 - t_s\alpha_1)(1 - t_s\alpha_0)]T_o + t_s\beta[(1 - t_s\alpha_1)u_0 + u_1]\\
&\quad + [(1 - t_s\alpha_1)t_s\gamma_0 + t_s\gamma_1],\\
T_3 &= [(1 - t_s\alpha_2)(1 - t_s\alpha_1)(1 - t_s\alpha_0)]T_o\\
&\quad + t_s\beta[(1 - t_s\alpha_2)(1 - t_s\alpha_1)u_0 + (1 - t_s\alpha_2)u_1 + u_2]\\
&\quad + [(1 - t_s\alpha_2)(1 - t_s\alpha_1)t_s\gamma_0 + (1 - t_s\alpha_2)t_s\gamma_1 + t_s\gamma_2],\\
&\vdots\\
T_{k+1} &= T_o\prod_{j=0}^{k}(1 - t_s\alpha_j) + t_s\beta\sum_{j=0}^{k}u_j\prod_{i=j+1}^{k}(1 - t_s\alpha_i)\\
&\quad + \sum_{j=0}^{k}t_s\gamma_j\prod_{i=j+1}^{k}(1 - t_s\alpha_i),
\end{aligned} \tag{24}$$

where T_o and T_k are the initial and k-th water temperatures inside the tank respectively. t_s is the sampling time, whereas u_k is the k-th switch status, which is either 1or 0. α_j and γ_j are functions of Eqs. (8) and (10) respectively and β represents a constant given Eq. (9). The acceptable hot water temperature set points are given by inequality (25):

$$T_{low} \leqslant T_k \leqslant T_{up}, \tag{25}$$

where, T_{low} and T_{up} are the lower and upper desired temperatures respectively.

2.9. Objective function

The multi-objective function consists of energy cost, $w_1 t_s\sum_{k=1}^{N}P_{g,k}\lambda_k$, minimization and maximization of FC usage, $w_2 t_s\sum_{k=1}^{N}P_{FC-IN,k}$, in discrete time with weighting factors, w_1 and w_2. The objective function is normalized to level the sensitivity of the weighting factor by dividing the grid power variable by 1000 units. The control horizon is 24 h, with t_s being the sampling time, and the sampling interval is $(1 \leqslant k \leqslant N)$ whereas λ_k is the TOU tariff. N is the final sampling point.

The objective function is expressed as follows:

$$J = \frac{1}{1000}w_1 t_s\sum_{k=1}^{N}P_{g,k}\lambda_k - w_2 t_s\sum_{k=1}^{N}P_{FC-IN,k}, \tag{26}$$

subject to:

$$P_{el,k} + P_{RE-IN,k}/\eta_{in} = P_{w,k}\eta_w + P_{pv,k}\eta_{pv}, \tag{27}$$

$$P_{g,k} + P_{RE-IN,k} + P_{FC-IN,k} = P_{\text{Load},k} + P_{hp,k}u_k, \tag{28}$$

$$P_{el,k}\eta_{el} = P_{H2,k}, \tag{29}$$

$$P_{FC-IN,k} = \eta_{FC}P_{FC,k}, \tag{30}$$

$$\begin{aligned}
T_{low} \leqslant\ & T_o\prod_{j=0}^{k}(1 - t_s\alpha_j) + t_s\beta\sum_{j=0}^{k}u_j\prod_{i=j+1}^{k}(1 - t_s\alpha_i)\\
&+ \sum_{j=0}^{k}t_s\gamma_j\prod_{i=j+1}^{k}(1 - t_s\alpha_i) \leqslant T_{up},
\end{aligned} \tag{31}$$

$$E^{min} \leqslant E_s(0) + \sum_{\tau=1}^{k}P_{H2,\tau}t_s - \frac{1}{\eta_s}\sum_{\tau=1}^{k}P_{FC,\tau}t_s \leqslant E^{max}, \tag{32}$$

$$P_w = \begin{cases} P_r\frac{V^\chi - V_{in}^\chi}{V_r^\chi - V_{in}^\chi}, & (V_{in} \leqslant V \leqslant V_r)\\ P_r, & (V_r \leqslant V \leqslant V_{out})\\ 0, & (0 \leqslant V_{in}\text{and}V \leqslant V_{out}) \end{cases} \tag{33}$$

$$u_k \in \{0, 1\}. \tag{34}$$

where λ_k is the TOU electricity tariff (*R*/kWh) at the k-th sampling interval given in Eq. (20). Eq. (27) represents the power balance from the renewable sources which include power from wind and PV at any given sampling interval. This RE power is used to run the electrolyzer and the loads. Whereas Eq. (28) represents the power balance of the entire system, that is, power from the grid and RE is used to power the HPWH and the load. Eq. (33) is the wind generator power output characteristics, based on wind speed. Eqs. (29) and (30) represent the FCs' power balances with their respective inverters. The two state variables, that is, hot water temperature and hydrogen gas are given in inequalities (31) and (32) respectively. Finally, Eq. (34) is a binary switch control variable assuming only value of either 0 or 1, while the other control variables; $P_{RE-IN,k}, P_{el,k}, P_{H2,k}, P_{FC,k}, P_{FC-IN,k}, P_{g,k}$ are continuous real number.

2.10. Algorithm formulation in MATLAB

The OC problem is solved using SCIP algorithm in *OPTI toolbox* in MATLAB.

The matrix formulation of the objective function is divided into cost and energy function respectively:

For grid energy cost minimization J_e:

$$\begin{aligned}
J_e = f^T\mathbf{X} =\ & [0\ldots0_N, \lambda_1\ldots\lambda_N, 0\ldots0_N, 0\ldots0_N, 0\ldots0_N, 0\ldots0_N]_{1\times6N}\\
&\times [u_1\ldots u_N, P_{g,1}\ldots P_{g,N}, P_{RE-IN,1}\ldots P_{RE-IN,N}, P_{H2,1}\ldots P_{H2,N},\\
&P_{FC-IN,1}\ldots P_{FC-IN,N}, P_{FC,1}\ldots P_{FC,N}]'_{6N\times1},
\end{aligned} \tag{35}$$

for FC power output maximization J_{FC}:

$$\begin{aligned}
J_{FC} = f^T\mathbf{X} =\ & [0\ldots0_N, 0\ldots0_N, 0\ldots0_N, 0\ldots0_N, 1\ldots1_N, 0\ldots0_N]_{1\times6N}\\
&\times [u_1\ldots u_N, P_{g,1}\ldots P_{g,N}, P_{RE-IN,1}\ldots P_{RE-IN,N}, P_{H2,1}\ldots P_{H2,N},\\
&P_{FC-IN,1}\ldots P_{FC-IN,N}, P_{FC,1}\ldots P_{FC,N}]'_{6N\times1}.
\end{aligned} \tag{36}$$

Finally the multi-objective function is:

$$minJ = t_s w_1 \sum_{k=1}^{N} J_e - t_s w_2 \sum_{k=1}^{N} J_{FC}, \tag{37}$$

subject to

$$\begin{aligned} \mathbf{AX} &\leqslant \mathbf{b} \quad \text{(linear inequality constraint)}, \\ \mathbf{A_{eq}X} &= \mathbf{b_{eq}} \quad \text{(linear equality constraint)}. \end{aligned} \tag{38}$$

The detailed formulation of the above constraints are given in Appendix A.

3. Simulation results and discussion

3.1. Case study

The case study is done on a facility in Pretoria, South Africa. This facility intends to be a positive-energy building; the installation of wind, PV and FCs generator is under way. The current control strategy on these equipment is a proportional integral derivative (PID) controller incapable of handling hard constraints and on-line optimization. The baseline situation at the facility is that grid power supplies all the loads. Therefore, this paper proposes an OC strategy incorporating RE sources and FCs at this facility. The sampling time $t_s = 30$ min, while $N = 48$ and the control horizon is 24 h.

Because of the difficulties of consolidated input data of this facility, the relatively similar data are adopted from Sichilalu et al. (2015). The inlet cold water temperature and hot water demand are shown in Fig. 2:

3.1.1. Heat pump water heater parameters

The HPWH considered in this paper is a Quantum solar heat pump[3] air source tank-wrapped heat exchanger (condenser) and its parameters are shown in Table 1. The preferred hot water temperature is set to 55 °C $\leqslant T_k \leqslant$ 60 °C; the average country ambient temperature of $T_a = 25$ °C is used. The initial water temperature in the tank is set to $T_o = 57$ °C. However, the above desirable temperature varies from one individual to another.

3.1.2. Wind generator parameters

The wind generator in the case study is a Ruam Energy[4] turbine with technical specifications given in Table 2. The parameters are given in Table 2:

The wind turbine revolution per minute (RPM) rate is 280 RPM. The hourly measured wind and hub height speeds are shown in Fig. 3:

3.1.3. Photovoltaic power generation

The PV power is input data in this model, taken from our previous research (Sichilalu and Xia, 2015; Tazvinga et al., 2013) on the data measured on an installed facility in South Africa. The power output P_{pv} profile is given in Fig. 4 on the far right.

3.1.4. Inverter and fuel cell parameters

The FC under consideration is a stationary type with a wider application in commercial, industrial, and residential use, which can supplement the grid power supply. The electrolyzer efficiency is taken to be $\eta_{el} = 0.65$, hydrogen storage tank $\eta_s = 0.95$ and overall FC efficiency $\eta_{FC} = 0.5$. The hydrogen tank energy storage capacity has a minimum $E^{min} = 0$ kWh and maximum $E^{max} = 25$ kWh, the initial status of hydrogen energy is taken to be $E_s(0) = 3$ kWh, while all the inverters' efficiency both DC/DC and AC/DC or vice versa, is taken to be $\eta_{in} = 0.98$.

[3] http://www.quantumecohotwater.com.au.
[4] http://www.raumenergy.com.

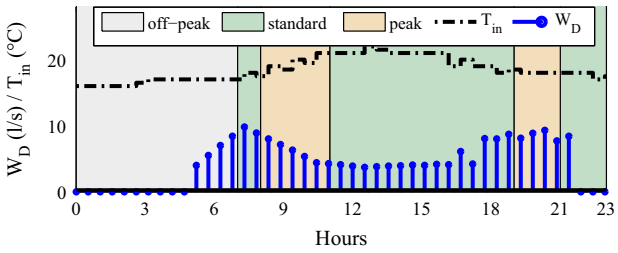

Fig. 2. Water demand flow rate and inlet cold water temperature.

3.2. Simulation results

The simulations are carried out to assess the feasibility and viability of implementing the proposed integrated FC hybrid system. Two simulation scenarios are analyzed: Case I without RE feed-in (export to the grid) and Case II, having RE energy feed-in. Case I is important in remote areas and off-grid locations, where this model is the only source of power. While case II, is applicable for grid connected systems. These two scenarios helps to analyze the operational robustness of this proposed model in order to account for all the possible applications.

Case I

3.2.1. Optimal power control strategy of a fuel cell hybrid system

The optimal power scheduling strategy of the FC-grid-RE integrated system is shown in Fig. 4. The weighting factors are set to $w_1 = 0.7$ and $w_2 = 0.3$, giving more weight on the minimization of grid energy. In Fig. 4, the grid P_g meets all domestic load P_{load} and heat pump P_{hp} from 00:00 till 07:00 at the end of the morning off-peak TOU period, since of wind energy P_w and PV P_{pv} are unavailable. There is no P_w generation in this period because the wind velocities are below cut-in speed on this simulated day. Though the FC has an initial status of energy $E_s(0) = 3$ kWh (Fig. 5), the OC opts to avoid its usage because of poor energy conversion efficiency. The OC instead uses the off-peak TOU grid energy. The OC strategy changes as the TOU enters the standard period at 07:00; the energy becomes slightly more expensive, the OC cuts off the grid supply to 0 kW and brings in 0.7 kW of RE power, P_{RE-IN}, to sustain the domestic load. In the same peak period P_{RE-IN} is insufficient to sustain the all the load, therefore FC, P_{FC-IN}, is operated feeding 0.12 kW at 07:00 and 1.22 kW at 08:00. Unfortunately, 5.15 kW of grid power is consumed when the heat pump switches *on* (in Fig. 6) at 8:00 in the peak period due to morning peak hot water demand averaging 8 l/s. The available FC and RE power cannot meet the demand and the grid comes into supply power for an hour. During the afternoon standard TOU the FC is not used to supply power; the wind, PV and grid meet the load. The cutting off of supply from the FC can only be attributed to its huge power losses in terms of efficiency whenever it operates.

The optimal strategy in Fig. 4, avoids using peak TOU energy as much as possible to save energy cost. The evening peak is mainly powered by the grid, FC and wind, since PV power is not available at night.

3.2.2. Fuel cell scheduling strategy and hydrogen storage dynamics

In Fig. 5 optimal FC power dispatch is shown. The power source of the electrolyzer is the RE supply to generate hydrogen. The FC power P_{PF-IN} supply is *off* from 00:00 to 07:30, the loads are supplied by the grid during the off-peak period. The stored hydrogen energy H_2 drops at 07:30 owing to the resumption of the FC operation. P_{FC-IN} supplies the load from 07:30 to 9:30 in the morning peak period. The stored hydrogen H_2, sharply declines to from

Table 1
Heat pump parameters and coefficients.

Power input (kW)	COP	Storage capacity (l)	Compressor (cc)	Tank (h/ø) (m)	Δx (m)	κ (W/m K)	h (W/m^2 K)
7	3.8	270	39.0	1.41 × 0.66	0.035	0.055	6.3

Table 2
Wind generator parameters and coefficients.

P_r (kW)	φ	h_{ref} (m)	h_{hub} (m)	χ	V_{in} (m/s)	V_r (m/s)	V_{out} (m/s)
7	1/7	10	30	2	2.0	11	50

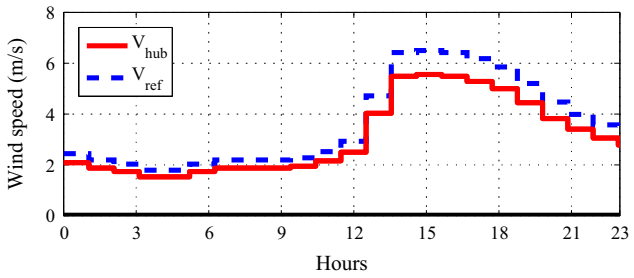

Fig. 3. Hub height and reference height wind speeds.

3 kW to 0.25 kW during this interval because the OC keeps the electrolyzer switched *off*, meanly because the hydrogen tank is not depleted. There is no hydrogen generation till 10:00 when the heat pump demand off, and the excess RE is then used is used to power the electrolyzer at 09:30 producing 0.30 kW hydrogen power and the hydrogen gas start building in the tank to the maximum of 2.81 kW. A steady increase in hydrogen storage is observed between 10:00 and 12:00. This is attributed to the low load demand. The OC again actuates the electrolyzer at 16:00 and hydrogen power P_{H2} production begins, further increasing the stored hydrogen. During the evening peak, the FC operates once again, as at this time only the FC has enough power reserve, since RE production has dwindled.

The OC avoids operating the FC at all times, the RE meanwhile can directly supply the loads treating the FC as storage system. The OC just operates it in peak period or when the RE is completely unavailable. However, depending on the desired effect, the weighting factor can be adjusted to make sure the fuel cell depletes all the stored hydrogen during operation. The OC opts to supply RE directly to the load instead of powering the electrolyzer to store RE energy in form of hydrogen gas. The OC restricts the operation of the FC due to poor efficiency. In Fig. 5, on the far right, the accumulative hydrogen mass plotted according to Eq. (17) is shown. The pressure drop inside the tank limits the complete utilization of hydrogen; because of this, lower and upper limit are given for each specified storage tank.

3.2.3. Thermal load switching control

In this model, the domestic load is deterministic at each sampling interval, the hot water demand is shown in Fig. 2. It is assumed that at any sampling time the heat pump operates at its full rated power demand of 7 kW. The lower and upper limits are set according to each individual's desired temperature range given in subSection 3.1. Fig. 6 shows the optimal switching u_k and the hot water state variable T_k of the heat pump. The heat pump switch u_k turns *on* around 04:00 for an hour and a corresponding rise in hot water temperature T_k till 58.72 °C is observed. From midnight to 04:30 when there is no hot water demand, a negligible drop in T_k is seen owing to the best heat pump insulation level. However, the preheated water temperature falls from 58.72 °C to 55.46 °C

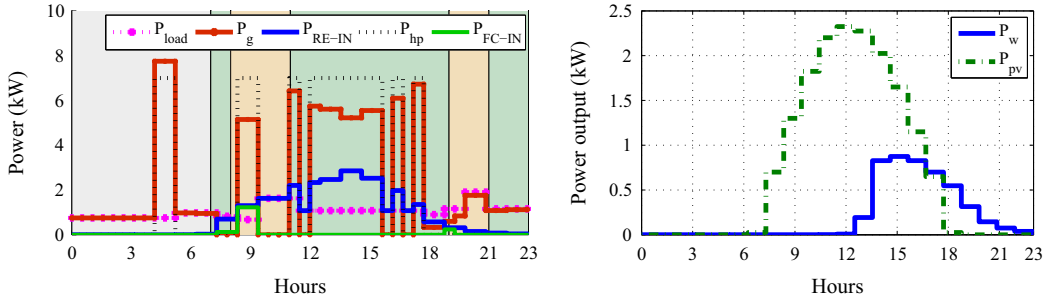

Fig. 4. Optimal power scheduling strategy and wind/PV power generation.

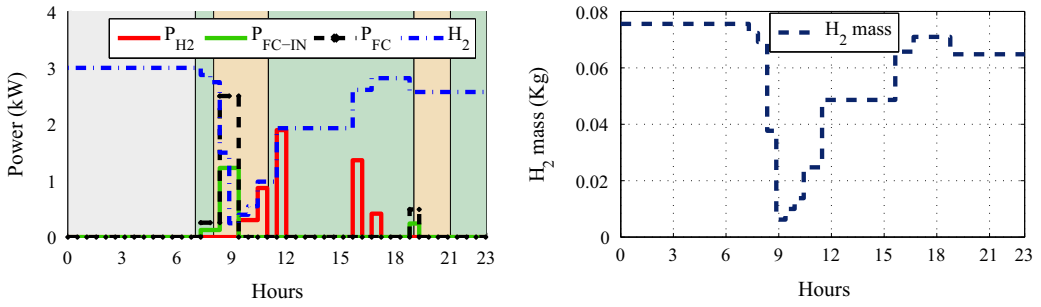

Fig. 5. Fuel cell optimal power dispatch and hydrogen gas mass.

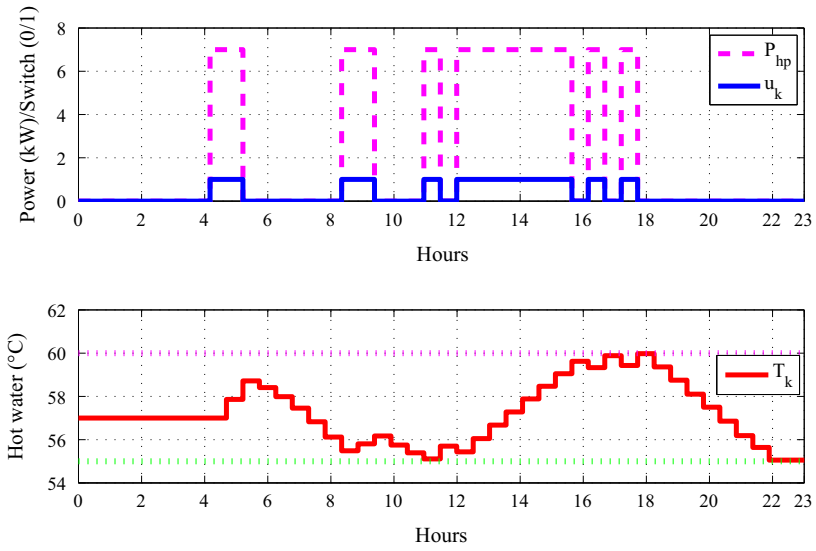

Fig. 6. Optimal heat pump switching strategy and hot water temperature T_k.

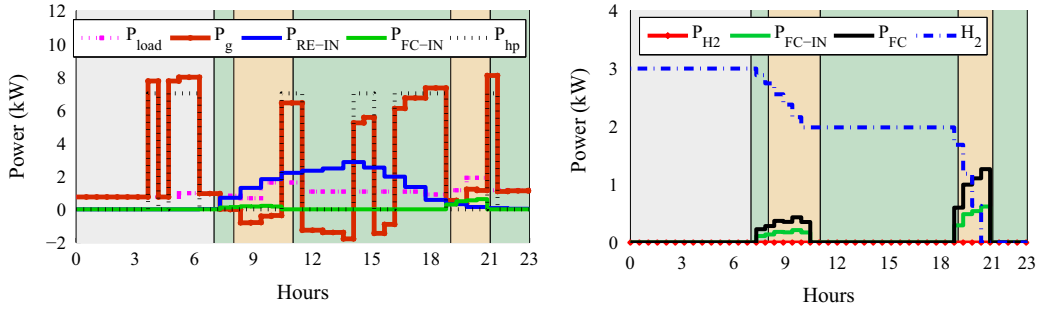

Fig. 7. Optimal power strategy during renewable power export mode into the grid.

during the morning hot water demand between 05:00 and 09:00. The OC switches *on* the heat pump again after 08:30 to heat the water that is almost hitting the lower set-point. The inlet cold water is the major cause of the temperature drop inside the tank, in addition to hot water demand. The OC operates the heat pump from 12:00 to 15:30 in readiness for the evening peak demand, thereby avoiding operating it in the evening peak period and thus making use of standard TOU that is relatively cheaper.

The heat pump water's temperature is highest to about 60 °C between 17:00 and 18:30, enough to meet the evening demand and that of the rest of the night. The proposed models show the capacity to optimally predict, control and meet the state variable water constraint. The hot water temperature set point bounds reflected in Fig. 6 are slightly too stringent, prompting the OC to increase the heat pump's switching u_k frequency.

Case II

3.2.4. Optimal feed-in power control strategy

The notable major difference between the two operational scenarios in Figs. 4 and 7 is that the OC does not use the electrolyzer at all in case II. The RE feed-in takes place between 08:30 and 10:30 feeding maximum power of 0.81 kW and later on between 11:30 and 14:00, feeding maximum power of approximately 1.78 kW. The feed-in happens only during the periods when the heat pump is not operational. The OC stops the feed-in during peak load, because all the generated RE is used to supplement the grid power, which is expensive to purchase.

The FC P_{FC-IN} is used twice during the peak period. This can be attributed to higher FC system power loss due to its low efficiency; the OC therefore, rather opts to sell RE power to the grid. The proposed model has shown greater capability of power control and can effectively improve the scheduling strategy of these systems, which are conventionally on programmable logic controllers or pro portional-integral-derivatives (PIDs). The OC technique maximizes operational efficiency based on the cost function.

3.3. Baseline and optimal control savings

The facility in the case study currently uses only the grid to sustain all the loads, here referred to as the baseline. The proposed intervention is the addition of wind, PV, FC and OC, referred to as the optimal situation. Table 3 shows the baseline/current and after implementation of the model, tabulating the predicted savings on a 24-h basis. The simulation results in Table 3 are for case I.

The energy saving is about 27.68% owing to the addition of the RE sources coupled with an optimal load-shifting strategy. The OC avoids using the power from the grid during standard and peak TOU electricity tariff, this significantly reduces the cost and

Table 3
Baseline and optimal energy/cost savings.

Baseline (kWh)	Baseline cost (R/day)	Optimal (kWh)	Optimal cost (R/day)	Energy saving (%)	Cost saving (%)
74.00	66.08	53.52	43.69	27.68	33.8

translates into lower grid energy cost of 33.8%. The proposed model has the potential of effecting savings for this facility in the case study, provided the REs rides on OC strategy instead of the traditional logical controllers. Though this paper does not look into economic analysis and the payback period, it could be interesting in future research to quantify these estimates. The proposed model opens the door for integration and OC of FCs with other distributed RE sources, especially in developing countries experiencing a power deficit (e.g. Zambia, Zimbabwe, South Africa).

4. Conclusions

An OC model of an integrated FC-RE-grid hybrid energy system with a thermal load meeting all the operation constraints has been presented. The OC is providing the required hot water demand and optimally schedules the RE system with FC mainly used as back-up/storage energy sources. The model can be used for feed-in and load shifting in order to minimize grid energy cost; it avoids operating the thermal load in the peak TOU period. The proposed model can effectively improve the operational and system efficiency, which results in minimization of energy losses. The engineering challenge facing RE and energy-efficient equipment integration has been solved in this paper, especially on DSM load-shifting strategy. The traditional control methods, such as a PID controller used in the operation of such hybrid system can be improved by OC strategy in the current energy mix and electricity market environment. This paper considered the open-loop control problem, though, it gives the precise predictions based on pre-focused input data, it is highly recommend in the future research to apply a closed-loop model predictive control (MPC) which can effectively counter the uncertainties associated with RE input parameters (e.g., wind speed and solar irradiance). Nonetheless, this open-loop optimal result based on a 24-h control horizon has a high prediction accuracy because all the hourly variation of input data is incorporated and simulated on each single day of the year. This model can be adopted for RE hybrid supply and feed-in on commercial or domestic buildings.

Acknowledgements

The authors thank the National Research Foundation (NRF) Grant No. 99766 South Africa, the University of Zambia, Council for Scientific and Industrial Research South Africa and the National Hub for Energy Efficiency and Demand Side Management for financial and other support for this research.

Appendix A. Algorithm formulation

The proposed model has a binary variable and real number control variables, solved using the *OPTI toolbox* SCIP algorithm in MATLAB.

A.1. Inequality matrices

The general formulation of the inequality constraint is shown in Eq. (A.1):

$$\mathbf{AX} \leqslant \mathbf{b}. \tag{A.1}$$

Vector $\mathbf{X}$ comprises all the control variables and they are given in matrix (A.2):

$$\mathbf{X} = \left[u_1 \dots u_N, P_{g,1} \dots P_{g,N}, P_{RE-IN,1} \dots P_{RE-IN,N}, P_{H2,1} \dots P_{H2,N}, P_{FC-IN,1} \dots P_{FC-IN,N}, P_{FC,1} \dots P_{FC,N}\right]'_{6N\times 1}. \tag{A.2}$$

The spacial matrix $\mathbf{A}$ and vector $\mathbf{b}$ are formulated as follows:

Let matrix $\mathbf{A_1}$ represent the state variable of the thermal load, shown in Eq. (A.3):

$$\mathbf{A_1} = t_s\beta \begin{bmatrix} 1 & 0 & 0 & 0 & \dots & 0 \\ (1-t_s\alpha_1) & 1 & 0 & 0 & \dots & 0 \\ (1-t_s\alpha_2)(1-t_s\alpha_1) & (1-t_s\alpha_2) & 1 & 0 & \dots & 0 \\ \vdots & \vdots & \vdots & \ddots & \vdots & \\ (1-t_s\alpha_{N-2})\times\dots\times(1-t_s\alpha_1) & (1-t_s\alpha_{N-2})\times\dots\times(1-t_s\alpha_2) & \dots & \dots & 1 & 0 \\ (1-t_s\alpha_{N-1})(1-t_s\alpha_{N-2})\times\dots\times(1-t_s\alpha_1) & (1-t_s\alpha_{N-1})\times\dots\times(1-t_s\alpha_2) & \dots & \dots & (1-t_s\alpha_{N-1}) & 1 \end{bmatrix}_{N\times N}, \tag{A.3}$$

The $2N \times 6N$ matrix below represent a combined inequality (A.3) and the FC status of energy inequality (32), in this appendix each sub-matrix inside the bigger matrix is an $N \times N$ dimension:

$$\mathbf{A_2} = \left[\begin{array}{c|c|c|c|c|c} \mathbf{A_1} & 0\dots0 & 0\dots0 & 0\dots0 & 0\dots0 & 0\dots0 \\ & \vdots & \vdots & \vdots & \vdots & \vdots \\ & 0\dots0 & 0\dots0 & 0\dots0 & 0\dots0 & 0\dots0 \\ \hline 0\dots0 & 0\dots0 & 0\dots0 & t_s\dots0 & 0\dots0 & -\frac{t_s}{\eta_s}\dots0 \\ \vdots & \vdots & \vdots & \ddots & \vdots & \ddots \\ 0\dots0 & 0\dots0 & 0\dots0 & 0\dots t_s & 0\dots0 & -\frac{t_s}{\eta_b}\dots-\frac{t_s}{\eta_s} \end{array}\right]_{2N\times 6N}, \tag{A.4}$$

inequality (31) is reformulated into inequality (A.5) and inequality (A.6):

$$t_s\beta\sum_{j=0}^{k}u_j\prod_{i=j+1}^{k}(1-t_s\alpha_i) \leqslant T_{up} - T_o\prod_{j=0}^{k}(1-t_s\alpha_j) - \sum_{j=0}^{k}t_s\gamma_j\prod_{i=j+1}^{k}(1-t_s\alpha_i), \tag{A.5}$$

$$-t_s\beta\sum_{j=0}^{k}u_j\prod_{i=j+1}^{k}(1-t_s\alpha_i) \leqslant -T_{low} + T_o\prod_{j=0}^{k}(1-t_s\alpha_j) + \sum_{j=0}^{k}t_s\gamma_j\prod_{i=j+1}^{k}(1-t_s\alpha_i). \tag{A.6}$$

According to inequality (A.5) and inequality (A.6), the element of vectors $\mathbf{b_1}$ and $\mathbf{b_2}$ is:

$$b_{1,k} = T_{up} - T_o\prod_{j=0}^{k}(1-t_s\alpha_j) - \sum_{j=0}^{k}t_s\gamma_j\prod_{i=j+1}^{k}(1-t_s\alpha_i), \tag{A.7}$$

$$b_{2,k} = -T_{low} + T_o\prod_{j=0}^{k}(1-t_s\alpha_j) + \sum_{j=0}^{k}t_s\gamma_j\prod_{i=j+1}^{k}(1-t_s\alpha_i). \tag{A.8}$$

Vector $\mathbf{b_1}$ in Eq. (A.7) is the difference of the three vectors $\mathbf{b_3}$, $\mathbf{b_4}$ and $\mathbf{b_5}$, as shown in Eq. (A.9).

$$\mathbf{b_1} = \mathbf{b_3} - \mathbf{b_4} - \mathbf{b_5}, \tag{A.9}$$

where,

$$\mathbf{b_3} = \begin{bmatrix} T_{up} \\ \vdots \\ T_{up} \end{bmatrix}_{N\times 1}, \tag{A.10}$$

then vector $\mathbf{b_4}$ is given in Eq. (A.11),

$$\mathbf{b_4} = T_o = \begin{bmatrix} (1-t_s\alpha_0) \\ (1-t_s\alpha_1)(1-t_s\alpha_0) \\ (1-t_s\alpha_2)(1-t_s\alpha_1)(1-t_s\alpha_0) \\ \vdots \\ (1-t_s\alpha_{N-2})(1-t_s\alpha_{N-3})\times\ldots\times(1-t_s\alpha_0) \\ (1-t_s\alpha_{N-1})(1-t_s\alpha_{N-2})(1-t_s\alpha_{N-3})\times\ldots\times(1-t_s\alpha_0) \end{bmatrix}_{N\times 1}, \tag{A.11}$$

and finally, $\mathbf{b_5}$ is given in Eq. (A.12) below,

$$\mathbf{b_5} = \begin{bmatrix} t_s\gamma_o \\ (1-t_s\alpha_1)t_s\gamma_o + t_s\gamma_1 \\ (1-t_s\alpha_2)(1-t_s\alpha_1)t_s\gamma_o + (1-t_s\alpha_2)t_s\gamma_1 + t_s\gamma_2 \\ \vdots \\ (1-t_s\alpha_{N-2})\times\ldots\times(1-t_s\alpha_1)t_s\gamma_o + (1-t_s\alpha_{N-2})\times\ldots\times(1-t_s\alpha_2)t_s\gamma_1 + \ldots + t_s\gamma_{N-2} \\ (1-t_s\alpha_{N-1})(1-t_s\alpha_{N-2})\times\ldots\times(1-t_s\alpha_1)t_s\gamma_o + (1-t_s\alpha_{N-1})\times\ldots\times(1-t_s\alpha_2)t_s\gamma_1 + \ldots(1-t_s\alpha_{N-1})t_s\gamma_{N-2} + t_s\gamma_{N-1} \end{bmatrix}. \tag{A.12}$$

The T_{low} vector is given in Eq. (A.13), the formulation of the $\mathbf{b_2}$ vector is analogous to $\mathbf{b_1}$ given in Eq. (A.14),

$$\mathbf{b_6} = \begin{bmatrix} T_{low} \\ \vdots \\ T_{low} \end{bmatrix}_{N\times 1}, \tag{A.13}$$

$$\mathbf{b_2} = -\mathbf{b_6} + \mathbf{b_4} + \mathbf{b_5}. \tag{A.14}$$

Finally, the FC vectors are given in matrix (A.15) and (A.16) for the maximum and minimum hydrogen storage capacity respectively:

$$\mathbf{b_7} = \begin{bmatrix} E^{max} - E(0) \\ \vdots \\ E^{max} - E(0) \end{bmatrix}_{N\times 1}, \tag{A.15}$$

$$\mathbf{b_8} = \begin{bmatrix} -E^{min} + E(0) \\ \vdots \\ -E^{min} + E(0) \end{bmatrix}_{N\times 1}. \tag{A.16}$$

The final inequality **A** matrices and vector **b** are given in (A.17) and (A.18) respectively.

$$\mathbf{A} = \begin{bmatrix} \mathbf{A_2} \\ -\mathbf{A_2} \end{bmatrix}_{4N\times 6N}, \tag{A.17}$$

$$\mathbf{B} = \begin{bmatrix} \mathbf{b_1} \\ \mathbf{b_7} \\ \mathbf{b_2} \\ \mathbf{b_8} \end{bmatrix}_{4N\times 1}, \tag{A.18}$$

A.2. Equality matrices

The power balance equality constraint in Eqs. (27), (28) and (30), are sparse matrix $\mathbf{A_{eq}}$, given in Eq. (A.19):

$$\mathbf{A_{eq}} = \left[\begin{array}{cccccc} 0\ldots0 & 0\ldots0 & \eta_{in}\ldots0 & \eta_{el}\ldots0 & 0\ldots0 & 0\ldots0 \\ \vdots & \vdots & \ddots & \ddots & \vdots & \vdots \\ 0\ldots0 & 0\ldots0 & 0\ldots\eta_{in} & 0\ldots\eta_{el} & 0\ldots0 & 0\ldots0 \\ \hline -P_{hp}\ldots0 & 1\ldots0 & 1\ldots0 & 0\ldots0 & 1\ldots0 & 0\ldots0 \\ \ddots & \ddots & \ddots & \vdots & \ddots & \vdots \\ 0\ldots-P_{hp} & 0\ldots1 & 0\ldots1 & 0\ldots0 & 0\ldots1 & 0\ldots0 \\ \hline 0\ldots0 & 0\ldots0 & 0\ldots0 & 0\ldots0 & -1\ldots0 & \eta_{FC}\eta_{in}\ldots0 \\ \vdots & \vdots & \vdots & \vdots & \ddots & \ddots \\ 0\ldots0 & 0\ldots0 & 0\ldots0 & 0\ldots0 & 0\ldots-1 & 0\ldots\eta_{FC}\eta_{in} \end{array}\right]_{3N\times 6N}, \tag{A.19}$$

The k-th total PV power, wind power and the demand constitute the elements of vector $\mathbf{b_{eq}}$ is shown in Eq. (A.20):

$$\mathbf{b_{eq}} = \begin{bmatrix} \eta_w P_{w,1} + \eta_{pv} P_{pv,1} \\ \vdots \\ \eta_w P_{w,N} + \eta_{pv} P_{pv,N} \\ \hline P_{load,1} \\ \vdots \\ P_{load,N} \\ \hline 0 \\ \vdots \\ 0 \end{bmatrix}_{3N\times 1}. \tag{A.20}$$

The canonical form is $\mathbf{A_{eq}X} = \mathbf{b_{eq}}$ where $\mathbf{A_{eq}}$ is given in Eq. (A.19) and $\mathbf{b_{eq}}$ in Eq. (A.20).

The limits of the control variables are restricted between the lower and upper bounds, given in Eqs. (A.21) and (A.22):

lower bounds

$$lb^T = \left[0_1\ldots0_N, -\infty_1\ldots-\infty_N, 0_1\ldots0_N, E^{min}\ldots E^{min}, 0_1\ldots0_N, 0_1\ldots0_N\right]_{6N\times 1}, \tag{A.21}$$

upper bounds

$$ub^T = \left[1_1\ldots1_N, \infty_1\ldots\infty_N, P^{rated}_{RE-IN,1}\ldots P^{rated}_{RE-IN,N}, E^{max}\ldots E^{max}, P^{rated}_{FC-IN,1}\ldots P^{rated}_{FC-IN,N}, P^{rated}_{FC,1}\ldots P^{rated}_{FC,N}\right]_{6N\times 1}. \tag{A.22}$$

References

Arteconi, A., Hewitt, N., Polonara, F., 2013. Domestic demand-side management (DSM): Role of heat pumps and thermal energy storage (TES) systems. Appl. Therm. Eng. 51 (1), 155–165.

Ashok, S., 2007. Optimised model for community-based hybrid energy system. Renew. Energy 32 (7), 1155–1164.

Belfkira, R., Zhang, L., Barakat, G., 2011. Optimal sizing study of hybrid wind/PV/diesel power generation unit. Sol. Energy 85 (1), 100–110.
Bizon, N., Oproescu, M., Raceanu, M., 2015. Efficient energy control strategies for a standalone renewable/fuel cell hybrid power source. Energy Convers. Manage. 90, 93–110.
Bouzerdoum, M., Mellit, A., Massi Pavan, A., 2013. A hybrid model (sarima–svm) for short-term power forecasting of a small-scale grid-connected photovoltaic plant. Sol. Energy 98, 226–235.
Bueno, C., Carta, J., 2005. Technical–economic analysis of wind-powered pumped hydrostorage systems. Part i: model development. Sol. Energy 78 (3), 382–395.
Choudar, A., Boukhetala, D., Barkat, S., Brucker, J.-M., 2015. A local energy management of a hybrid PV-storage based distributed generation for microgrids. Energy Convers. Manage. 90, 21–33.
Chow, T., Bai, Y., Fong, K., Lin, Z., 2012. Analysis of a solar assisted heat pump system for indoor swimming pool water and space heating. Appl. Energy 100, 309–317.
Chua, K., Chou, S., Yang, W., 2010. Advances in heat pump systems: a review. Appl. Energy 87 (12), 3611–3624.
Dolan, P., Nehrir, M., Gerez, V., 1996. Development of a Monte Carlo based aggregate model for residential electric water heater loads. Electric Power Syst. Res. 36 (1), 29–35.
Dufo-Lopez, R., Bernal-Agustin, J.L., Yusta-Loyo, J.M., Dominguez-Navarro, J., Ramirez-Rosado, I.J., Lujano, J., Aso, I., 2011. Multi-objective optimization minimizing cost and life cycle emissions of stand-alone PV–wind–diesel systems with batteries storage. Appl. Energy 88 (11), 4033–4041.
Ellis, M., von Spakovsky, M., Nelson, D., 2001. Fuel cell systems: efficient, flexible energy conversion for the 21st century, vol. 89, p. 1808–1818. doi:http://dx.doi.org/10.1109/5.975914.
Fabrizio, E., Seguro, F., Filippi, M., 2014. Integrated HVAC and DHW production systems for zero energy buildings. Renew. Sustain. Energy Rev. 40, 515–541.
Feng, X., Gooi, H.B., Chen, S., 2015. Capacity fade-based energy management for lithium-ion batteries used in PV systems. Electric Power Syst. Res. 129, 150–159.
Gustafson, M., Baylor, J., Epstein, G., 1993. Direct water heater load control-estimating program effectiveness using an engineering model. IEEE Trans. Power Syst. 8 (1), 137–143.
Hove, T., Tazvinga, H., 2012. A techno-economic model for optimising component sizing and energy dispatch strategy for PV-diesel-battery hybrid power systems. J. Energy Southern Africa 23 (4), 18–28.
Huang, W.Z., Zaheeruddin, M., Cho, S., 2006. Dynamic simulation of energy management control functions for HVAC systems in buildings. Energy Convers. Manage. 47 (7), 926–943.
Ji, J., Pei, G., Chow, T.-t., He, W., Zhang, A., Dong, J., Yi, H., 2005. Performance of multi-functional domestic heat-pump system. Appl. Energy 80 (3), 307–326.
Kaviani, A.K., Riahy, G., Kouhsari, S.M., 2009. Optimal design of a reliable hydrogen-based stand-alone wind/PV generating system, considering component outages. Renew. Energy 34 (11), 2380–2390.
Khan, K., Rasul, M., Khan, M.M.K., 2004. Energy conservation in buildings: cogeneration and cogeneration coupled with thermal energy storage. Appl. Energy 77 (1), 15–34.
Kilkis, Ì.B., 1999. Utilization of wind energy in space heating and cooling with hybrid HVAC systems and heat pumps. Energy Build. 30 (2), 147–153.
Kim, M., Kim, M.S., Chung, J.D., 2004. Transient thermal behavior of a water heater system driven by a heat pump. Int. J. Refrig. 27 (4), 415–421.
Korpås, M., Holen, A.T., 2006. Operation planning of hydrogen storage connected to wind power operating in a power market. IEEE Trans. Energy Convers. 21 (3), 742–749.
Li, H., Chen, Z., Polinder, H., 2009. Optimization of multibrid permanent-magnet wind generator systems. IEEE Trans. Energy Convers. 24 (1), 82–92.
Lu, L., Yang, H., Burnett, J., 2002. Investigation on wind power potential on Hong Kong islands: an analysis of wind power and wind turbine characteristics. Renew. Energy 27 (1), 1–12.
Patel, M.R., 2006. Wind and Solar Power Systems: Design, Analysis, and Operation. CRC Press, Boca Raton, FL.
Pukrushpan, J.T., Stefanopoulou, A.G., Peng, H., 2002. Modeling and control for pem fuel cell stack system. Proceedings of the American Control Conference, 2002, vol. 4. IEEE, pp. 3117–3122.
Pukrushpan, J.T., Stefanopoulou, A.G., Peng, H., 2004. Control of Fuel Cell Power Systems: Principles, Modeling, Analysis and Feedback Design. Springer Science & Business Media.
Purvins, A., Sumner, M., 2013. Optimal management of stationary lithium-ion battery system in electricity distribution grids. J. Power Sources 242, 742–755.
Rahman, M.M., Rasul, M., Khan, M.M.K., 2010. Energy conservation measures in an institutional building in sub-tropical climate in Australia. Appl. Energy 87 (10), 2994–3004.
Ranaboldo, M., Domenech, B., Reyes, G.A., Ferrer-Martí, L., Moreno, R.P., García-Villoria, A., 2015. Off-grid community electrification projects based on wind and solar energies: a case study in Nicaragua. Sol. Energy 117, 268–281.
Reihani, E., Sepasi, S., Roose, L.R., Matsuura, M., 2016. Energy management at the distribution grid using a battery energy storage system (BESS). Int. J. Electr. Power Energy Syst. 77, 337–344.
Rodatz, P., Paganelli, G., Sciarretta, A., Guzzella, L., 2005. Optimal power management of an experimental fuel cell/supercapacitor-powered hybrid vehicle. Control Eng. Pract. 13 (1), 41–53.
Roonprasang, N., Namprakai, P., Pratinthong, N., 2008. Experimental studies of a new solar water heater system using a solar water pump. Energy 33 (4), 639–646.
Rousseau, P., Greyvenstein, G., 2000. Enhancing the impact of heat pump water heaters in the South African commercial sector. Energy 25 (1), 51–70.
Safdarian, A., Ali, M., Fotuhi-Firuzabad, M., Lehtonen, M., 2016. Domestic EWH and HVAC management in smart grids: potential benefits and realization. Electric Power Syst. Res. 134, 38–46.
Seo, J., Ooka, R., Kim, J.T., Nam, Y., 2014. Optimization of the HVAC system design to minimize primary energy demand. Energy Build. 76, 102–108.
Sichilalu, S.M., Xia, X., 2015. Optimal energy control of grid tied PV–diesel–battery hybrid system powering heat pump water heater. Sol. Energy 115, 243–254.
Sichilalu, S., Mathaba, T., Xia, X., 2015. Optimal control of a wind-PV-hybrid powered heat pump water heater. Appl. Energy, doi:http://dx.doi.org/10.1016/j.apenergy.2015.10.072.
Singh, S., Singh, M., Chanana, S., Semwal, S., 2015. Frequency regulation of isolated hybrid wind/diesel, power generation with fuel cell system. In: Kamalakannan, C., Suresh, L.P., Dash, S.S., Panigrahi, B.K. (Eds.), Power Electronics and Renewable Energy Systems. Springer, India, pp. 853–862.
Tazvinga, H., Xia, X., Zhang, J., 2013. Minimum cost solution of photovoltaics-diesel-battery hybrid power systems for remote consumers. Sol. Energy 96, 292–299.
Tazvinga, H., Zhu, B., Xia, X., 2014. Energy dispatch strategy for a photovoltaic–wind–diesel–battery hybrid power system. Sol. Energy 108, 412–420.
Tazvinga, H., Zhu, B., Xia, X., 2015. Optimal power flow management for distributed energy resources with batteries. Energy Convers. Manage. 102, 104–110.
Verhelst, C., Degrauwe, D., Logist, F., Van Impe, J., Helsen, L., 2012. Multi-objective optimal control of an air-to-water heat pump for residential heating. Build. Simul. 5 (3), 281–291. http://dx.doi.org/10.1007/s12273-012-0061-z.
Wallmark, C., Alvfors, P., 2002. Design of stationary PEFC system configurations to meet heat and power demands. J. Power Sources 106 (1), 83–92.
Wang, Y., Wang, B., Chu, C.-C., Pota, H., Gadh, R., 2016. Energy management for a commercial building microgrid with stationary and mobile battery storage. Energy Build. 116, 141–150.
Zhang, J., Xia, X., 2007. Best switching time of hot water cylinder-switched optimal control approach. In: AFRICON 2007. IEEE, pp. 1–7.
Zhang, X., Zhao, X., Xu, J., Yu, X., 2013. Characterization of a solar photovoltaic/loop-heat-pipe heat pump water heating system. Appl. Energy 102, 1229–1245.